J|A|C|S
ARTICLES
Published on Web 02/22/2007

X-ray Scattering Study of Thin Films of Poly(2,5-bis(3-alkylthiophen-2-yl)thieno[3,2-*b*]thiophene)

Michael L. Chabinyc,*,† Michael F. Toney,‡ R. Joseph Kline,§ Iain McCulloch,|| and Martin Heeney||

Contribution from the Palo Alto Research Center, Palo Alto, California 94304, Stanford Synchrotron Research Laboratory, Stanford Linear Accelerator Center, Menlo Park, California 94025, Polymers Division, National Institute of Standards and Technology, Gaithersburg, Maryland 20899, and Merck Chemicals, Chilworth Science Park, Southampton, U.K.

Received October 5, 2006; E-mail: mchabinyc@parc.com

Abstract: Poly(2,5-bis(3-alkylthiophen-2-yl)thieno[3,2-*b*]thiophene), PBTTT, is a semiconducting polymer that forms thin film transistors (TFTs) with high field effect mobility on silicon dioxide dielectrics that are treated with alkyltrichlorosilanes (~0.2 to 0.5 cm^2/V s) but forms TFTs with poor mobility on bare silicon dioxide (<0.005 cm^2/V s). The microstructure of spin-coated thin films of PBTTT on these surfaces was studied using synchrotron X-ray diffraction and atomic force microscopy. PBTTT crystallizes with lamellae of π-stacked polymer chains on both surfaces. The crystalline domains are well-oriented relative to the substrate in the as-spun state and become highly oriented and more ordered with thermal annealing in the liquid crystalline mesophase. Although the X-ray scattering from PBTTT is nearly identical on both surfaces, atomic force microscopy showed that the domain size of the crystalline regions depends on the substrate surface. These results suggest that electrical transport in PBTTT films is strongly affected by the domain size of the crystalline regions and the disordered regions between them.

Introduction

Semiconducting polymers are important materials for the development of printed, mechanically flexible electronics such as flat panel displays[1,2] and photovoltaic cells.[3] Thin film transistors (TFTs) formed with active layers of thiophene-based polymers have been demonstrated with field-effect carrier mobilities of 0.1 to 0.5 cm^2/V s, values considered useful in many applications.[4−7] It is believed that molecular ordering in these materials is essential to the achievement of high carrier mobility because movement of charge relies on intermolecular electronic coupling. Despite this interest, relatively few detailed studies of how the microstructure of thin (<100 nm) films of semiconducting polymers varies with processing conditions, such as thermal annealing and interfacial interactions, have been reported.[5,8−23] Here we use X-ray scattering to determine how thermal annealing and interfacial interactions affect the molecular ordering and the orientation of crystalline domains in thin films of poly(2,5-bis(3-alkylthiophen-2-yl)thieno[3,2-*b*]thiophene), PBTTT (Figure 1).[6]

The majority of high performance, semiconducting polymers can be described as hairy, rigid-rod polymers, where the rod is the conjugated backbone and the hairs are the alkyl sidechains that solubilize the molecule.[24,25] The addition of alkyl side chains to rigid-rod polymers generally leads to hexagonal or lamellar

† Palo Alto Research Center.
‡ Stanford Linear Accelerator Center.
§ National Institute of Standards and Technology.
|| Merck Chemicals.

(1) Chabinyc, M. L.; Salleo, A. *Chem. Mater.* **2004**, *16*, 4509−4521.
(2) Crawford, G. P., Ed. *Flexible Flat Panel Displays*; John Wiley & Sons: New York, 2005.
(3) Coakley, K. M.; McGehee, M. D. *Chem. Mater.* **2004**, *16*, 4533−4542.
(4) Bao, Z.; Dodabalapur, A.; Lovinger, A. J. *Appl. Phys. Lett.* **1996**, *69*, 4108−4110.
(5) Sirringhaus, H.; Brown, P. J.; Friend, R. H.; Nielsen, M. M.; Bechgaard, K.; Langeveld-Voss, B. M. W.; Spiering, A. J. H.; Janssen, R. A. J.; Meijer, E. W.; Herwig, P.; De Leeuw, D. M. *Nature* **1999**, *401*, 685−688.
(6) McCulloch, I.; Heeney, M.; Bailey, C.; Genevicius, K.; Macdonald, I.; Shkunov, M.; Sparrowe, D.; Tierney, S.; Wagner, R.; Zhang, W.; Chabinyc, M. L.; Kline, R. J.; McGehee, M. D.; Toney, M. F. *Nat. Mater.* **2006**, *5*, 328−333.
(7) Ong, B. S.; Wu, Y.; Liu, P.; Gardner, S. *J. Am. Chem. Soc.* **2004**, *126*, 3378−3379.
(8) Kline, R. J.; McGehee, M. D.; Kadnikova, E. N.; Liu, J.; Frechet, J. M. J. *Adv. Mater.* **2003**, *15*, 1519−1522.
(9) Kline, R. J.; McGehee, M. D.; Kadnikova, E. N.; Liu, J.; Frechet, J. M. J.; Toney, M. F. *Macromolecules* **2005**, *38*, 3312−3319.
(10) Kline, R. J.; McGehee, M. D.; Toney, M. F. *Nat. Mater.* **2006**, *5*, 222−228.
(11) Kim, D. H.; Park, Y. D.; Jang, Y.; Yang, H.; Kim, Y. H.; Han, J. I.; Moon, D. G.; Park, S.; Chang, T.; Chang, C.; Joo, M.; Ryu, C. Y.; Cho, K. *Adv. Func. Mater.* **2005**, *15*, 77−82.
(12) Kawana, S.; Durrell, M.; Lu, J.; Macdonald, J. E.; Grell, M.; Bradley, D. D. C.; Jukes, P. C.; Jones, R. A. L.; Bennett, S. L. *Polymer* **2002**, *43*, 1907−1913.
(13) Aasmundveit, K. E.; Samuelsen, E. J.; Guldstein, M.; Steinsland, C.; Flornes, O.; Fagermo, C.; Seeberg, T. M.; Pettersson, L. A. A.; Inganas, O.; Reidenhans, R.; Ferrer, S. *Macromolecules* **2000**, *33*, 3120−3127.
(14) Knaapila, M.; Lyons, B. P.; Kisko, K.; Foreman, J. P.; Vaino, U.; Mihaylova, M.; Seeck, O. H.; Pallson, L.-O.; Serimaa, R.; Torkkeli, M.; Monkman, A. P. *J. Phys. Chem. B* **2003**, *107*, 12425−12430.
(15) Knaapila, M.; Kisko, K.; Lyons, B. P.; Stepanyan, R.; Foreman, J. P.; Seeck, O. H.; Vaino, U.; Pallson, L.-O.; Serimaa, R.; Torkkeli, M.; Monkman, A. P. *J. Phys. Chem. B* **2004**, *108*, 10711−10720.
(16) Knaapila, M.; Stepanyan, R.; Torkkeli, M.; Lyons, B. P.; Ikonen, T. P.; Almasy, L.; Foreman, J. P.; Serimaa, R.; Guntner, R.; Scherf, U.; Monkman, A. P.; Subbotin, A.; Ikkala, O.; ten Brinke, G. *Phys. Rev. E* **2005**, *71*, 041802.
(17) Olsen, B. D.; Jang, S.-Y.; Luning, J. M.; Segalman, R. A. *Macromolecules* **2006**, *39*, 4469−4479.
(18) Donley, C. L.; Zaumseil, J.; Andreasen, J. W.; Nielsen, M. M.; Sirringhaus, H.; Friend, R. H.; Kim, J.-S. *J. Am. Chem. Soc.* **2005**, *127*, 12890−12899.

10.1021/ja0670714 CCC: $37.00 **© 2007 American Chemical Society**

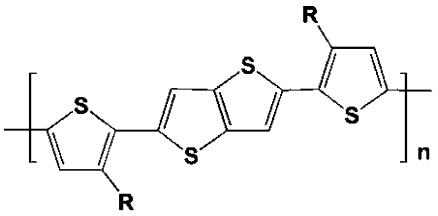

Figure 1. Repeat unit structure for poly(2,5-bis(3-alkylthiophen-2-yl)thieno-[3,2-*b*]thiophene), PBTTT.

packing schemes depending on the molecular structure of the backbone and the side chain.[26,27] Planar conjugated polymers with simple linear alkyl sidechains, such as poly(3-*n*-alkylthiophenes), adopt lamellar structures where there is efficient overlap of the π-orbitals of the backbone within each lamella (Figure 2).[28,29] This structure leads to highly anisotropic electrical transport; there is efficient electrical transport in two dimensions (along the backbone and through the π-stack) and relatively poor transport through the other dimension (the lamellar stack of insulating alkyl sidechains).[5,30] In thin-film electronic devices, it is therefore preferable to have the π-stacking or chain direction along the direction of the flow of current. Understanding how crystalline domains orient relative to the transport direction is therefore important to the correlation of electrical transport and molecular packing structure.

The microstructure of films of poly(alkylthiophenes), in particular poly(3-hexyl)thiophene (P3HT), have been extensively studied using X-ray scattering. X-ray scattering from thin films of P3HT is relatively weak, and few peaks are observed other than those due to lamellar stacking and to π-stacking.[5,9] It is difficult to quantitatively compare results from different studies as the microstructure in a film is strongly affected by the quality of material, e.g., polydispersity, the processing conditions, and interfacial interactions. The casting solvent, drying conditions, and thermal annealing steps can all have a major impact on the final microstructure of a film.[20,31−34] For example, near-edge X-ray fine absorption spectroscopy (NEXAFS) has been used

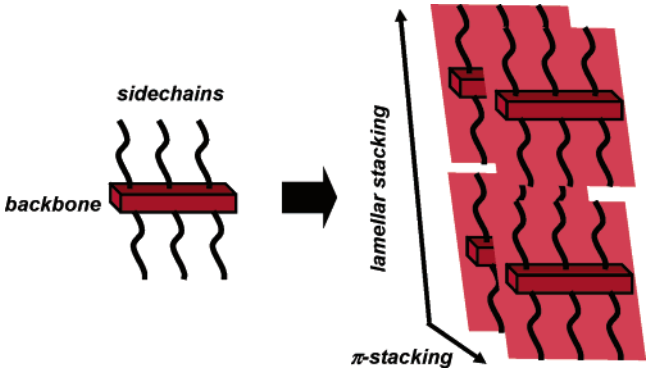

Figure 2. Schematic of lamellar and π-stacking for hairy, rigid-rod polymers.

to show that the orientation of polymer molecules in spun films of P3HT depend critically on the drying conditions used for casting the film.[33] Two populations of oriented domains, where the lamellar stacking direction is either perpendicular or parallel to the substrate, frequently coexist in films of P3HT.[5,9−11,13,19,20,35] In the majority of studies of thin films of highly regioregular P3HT (>95%), the dominant orientation of the crystalline domains is one where the lamellar stacking direction is along the surface normal.[5,8,9,11,19] It has been shown that the semicrystalline domains in thin films of P3HT can nucleate from the interface with the substrate; this observation demonstrates the importance of interfacial interactions on the microstructure of these films.[10] While most reports suggest that hydrophobic surfaces lead to preferential lamellar stacking perpendicular to the surface and that hydrophilic surfaces can lead to a mixture of orientations,[10] there are results suggesting that the preference is not absolute.[11]

We have recently reported initial characterization of PBTTT, describing its field-effect mobility, thermal properties, and crystalline structure. PBTTT currently exhibits the highest field effect mobility for a semiconducting polymer in thin-film transistors, ~0.5 cm^2/V s.[6] This value is attributed to the high degree of crystallinity in thin films of PBTTT that have domains with lamellar and π-stacked polymer chains (Figure 3). TFTs with the highest mobility are obtained with silicon dioxide dielectrics that have been coated with self-assembled monolayers (SAMs) formed from alkyltrichlorosilanes, such as octyltrichlorosilane (OTS).[36] Interestingly, TFTs made with bare SiO_2 gate dielectrics have a mobility that is ~100 times lower than those with OTS-SAMs (Figure 4). While it has been demonstrated that the microstructure of the semiconducting polymer at the interface has a strong influence on mobility,[37] it has also been suggested that interfacial traps or dipolar groups can also influence transport.[38] PBTTT is a good system to examine these effects due to its high crystallinity and electrical performance so we provide here the first detailed study of the microstructure of its thin films.

(19) Yang, H.; Shin, T. J.; Yang, L.; Cho, K.; Ryu, C. Y.; Bao, Z. *Adv. Funct. Mater.* **2005**, *15*, 671−676.
(20) Chang, J.-F.; Clark, J.; Zhao, N.; Sirringhaus, H.; Breiby, D. W.; Andreasen, J. W.; Nielsen, M. M.; GIles, M.; Heeney, M.; McCulloch, I. *Phys. Rev. B* **2006**, *74*, 115318.
(21) Zhang, R.; Li, B.; Iovu, M. C.; Jeffries-EL, M.; Sauvé, G.; Cooper, J.; Jia, S.; Stephanie Tristram-Nagle; Smilgies, D. M.; Lambeth, D. N.; McCullough, R. D.; Kowalewski, T. *J. Am. Chem. Soc.* **2006**, *128*, 3480−3481.
(22) Nagamutsu, S.; Takashima, W.; Kaneto, K.; Yoshida, Y.; Tanigaki, N.; Yase, K.; Omote, K. *Macromolecules* **2003**, *36*, 5252−5257.
(23) Misaki, M.; Ueda, Y.; Nagamatsu, S.; Yoshida, Y.; Tanigaki, N.; Yase, K. *Macromolecules* **2004**, *37*, 6926−6931.
(24) Ballauff, M. *Angew. Chem., Int. Ed. Engl.* **1989**, *28*, 253−267.
(25) Donald, A.; Windle, A.; Hanna, S. *Liquid Crystalline Polymers*, 2nd ed.; Cambridge University Press: Cambridge, 2006.
(26) Knaapila, M.; Stepanyan, R.; Lyons, B. P.; Torkkeli, M.; Monkman, A. P. *Adv. Funct. Mater.* **2006**, *16*, 599−609.
(27) Watanabe, J.; Harkness, B. R.; Sone, M.; Ichimura, H. *Macromolecules* **1994**, *27*, 507−512.
(28) Prosa, T. J.; Winokur, M. J.; Moulton, J.; Smith, P.; Heeger, A. J. *Macromolecules* **1992**, *25*, 4364−4372.
(29) McCullough, R. D. *Adv. Mater.* **1998**, *10*, 1−24.
(30) Österbacka, R.; An, C. P.; Jiang, X. M.; Vardeny, Z. V. *Science* **2000**, *287*, 839−842.
(31) Banach, M. J.; Friend, R. H.; Sirringhaus, H. *Macromolecules* **2004**, *37*, 6079−6085.
(32) Chang, J.-F.; Sun, B.; Breiby, D. W.; Nielsen, M. M.; Solling, T. I.; Giles, M.; McCulloch, I.; Sirringhaus, H. *Chem. Mater.* **2004**, *16*, 4772−4776.
(33) DeLongchamp, D. M.; Vogel, B. M.; Jung, Y.; Gurau, M. C.; Richter, C. A.; Kirillov, O. A.; Obrzut, J.; Fischer, D. A.; Sambasivan, S.; Richter, L. J.; Lin, E. K. *Chem. Mater.* **2005**, *17*, 5610−5612.
(34) Zhao, N.; Botton, G. A.; Zhu, S.; Duft, A.; Ong, B. S.; Wu, Y.; Liu, P. *Macromolecules* **2004**, *37*, 8307−8312.
(35) Zen, A.; Pflaum, J.; Hirschmann, S.; Zhuang, W.; Jaiser, F.; Asawapiron, U.; Rabe, J. P.; Scherf, U.; Neher, D. *Adv. Funct. Mater.* **2004**, *14*, 757−764.
(36) Kline, R. J.; DeLongchamp, D. M.; Fischer, D. A.; Lin, E. K.; Heeney, M.; McCulloch, I.; Toney, M. F. Submitted.
(37) Chabinyc, M. L.; Salleo, A.; Wu, Y.; Liu, P.; Ong, B. S.; Heeney, M.; McCulloch, I. *J. Am. Chem. Soc.* **2004**, *126*, 13928−13929.
(38) Veres, J.; Ogier, S. D.; Leeming, S. W.; Cupertino, D. C.; Khaffaf, S. M. *Adv. Funct. Mater.* **2003**, *13*, 199−204.

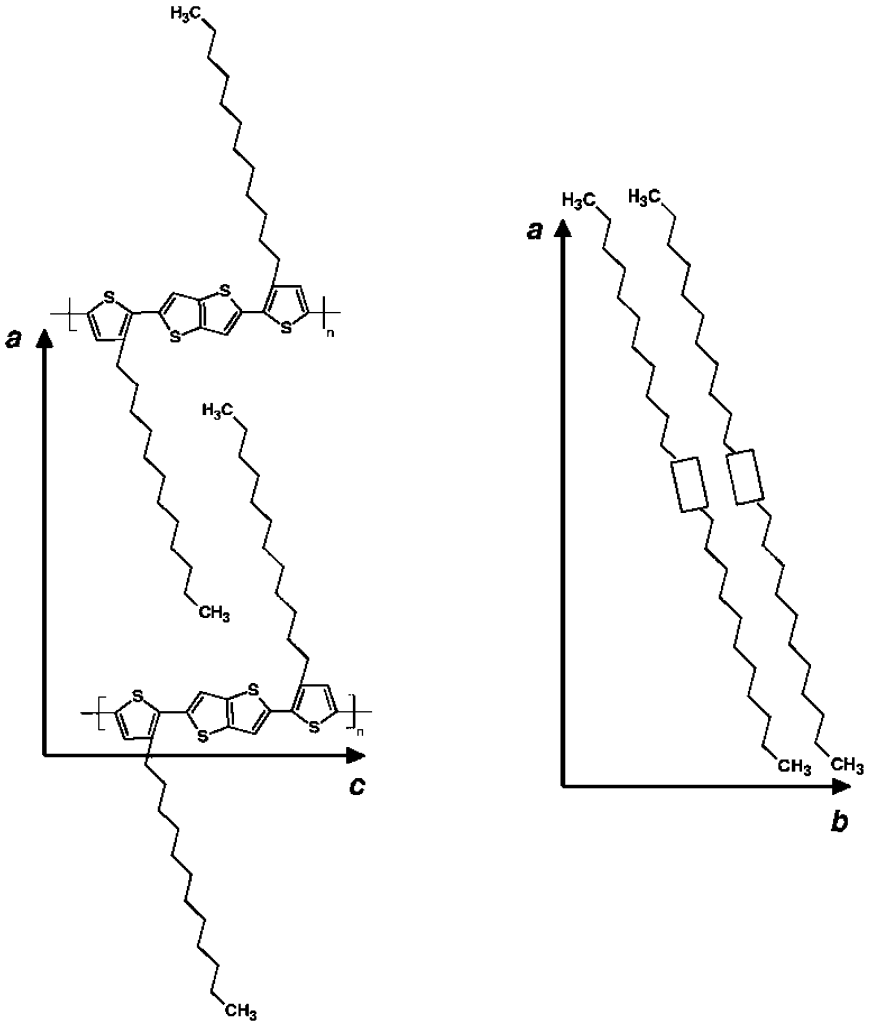

Figure 3. Schematic of molecular packing of PBTTT based on data from X-ray scattering. Lamellar stacking due to the alkyl side chains occurs along the *a*-axis, and π-stacking occurs along the *b*-axis. The positions of the molecules in the cell are qualitative and are not meant to quantitatively describe the details of the molecular packing, e.g., the extent of interdigitation of the sidechains.

Experimental Section

Materials. PBTTT was synthesized as described previously.[6] The molecular weight (MW) of the C12 materials was either 43 000 g/mol with a polydispersity (*D*) of 1.9 or 51 000 g/mol with a *D* of 1.85, and that of the C14 was 62 000 g/mol with a *D* of 2.2. No significant differences were noticed between the two batches of C12. Molecular weights were determined by gel permeation chromatography in chlorobenzene against polystyrene standards and are likely an overestimate of the true molecular weight.[39] The polymers were dissolved in 1,2-dicholorbenzene (~10 mg/mL) and filtered hot with a 1 μm PTFE syringe filter prior to spin coating.

Fabrication of Films. Thin films of PBTTT were spin-coated at 1000 rpm onto silicon wafers with a thin native oxide layer. The substrates were exposed to a low power oxygen plasma prior to spin-coating the PBTTT film. On some substrates, a self-assembled monolayer (SAM) of octyltrichlorosilane (OTS), was formed on the oxide using a previously reported procedure (OTS/SiO_2).[40] The resulting PBTTT films were ~70−100 nm in thickness. Films were thermally annealed on a hot plate either in the ambient or under nitrogen and cooled to room temperature by placement on a cool surface.

X-ray Scattering Measurements. Measurements of X-ray scattering were performed at the Stanford Synchrotron Radiation Laboratory on beamlines 2-1 (high-resolution specular scattering), 7-2 (high-resolution grazing incidence scattering with a point detector), and 11-3 (2-D scattering with an area detector, MAR345 image plate, at grazing and specular incidence). Data are expressed as a function of the scattering vector, **q**, that has a magnitude of $(4\pi/\lambda)\sin\theta$, where θ is half the scattering angle and λ is the wavelength of the incident radiation; the *d*-spacing of a peak is simply $2\pi/q$.[41] The incident energy was 8 keV for beam lines 2-1 and 7-2 and 12.7 keV for 11-3. The samples were kept under a helium atmosphere during irradiation to minimize damage to the films from the intense X-ray beam. Typical exposure times for the area detector measurements were 20−30 min. The data for out-of-plane scattering was corrected for the area of illumination by multiplication by θ, the incident angle. For the grazing incidence X-ray scattering (GIXS), the films were illuminated at an incidence angle of about 0.2° for 8 keV (7-2 measurements) and about 0.12° for 12.7 keV (11-3 measurements). These values were chosen so that the X-ray beam penetrates the entire thickness of the polymer sample (~100 nm) but only a portion (<20 nm) of the silicon substrate. This choice also reduces the background scattering from the substrate. The high-resolution GIXS data were corrected for the area of illumination based

(39) Grell, M.; Bradley, D. D. C.; Long, X.; Chamberlain, T.; Inbasekaran, M.; Woo, E. P.; Soliman, M. *Acta Polym.* **1998**, *49*, 439−444.
(40) Salleo, A.; Chabinyc, M. L.; Yang, M. S.; Street, R. A. *Appl. Phys. Lett.* **2002**, *81*, 4383−4385.
(41) Factor, B. J.; Russell, T. P.; Toney, M. F. *Macromolecules* **1993**, *26*, 2847−2859.

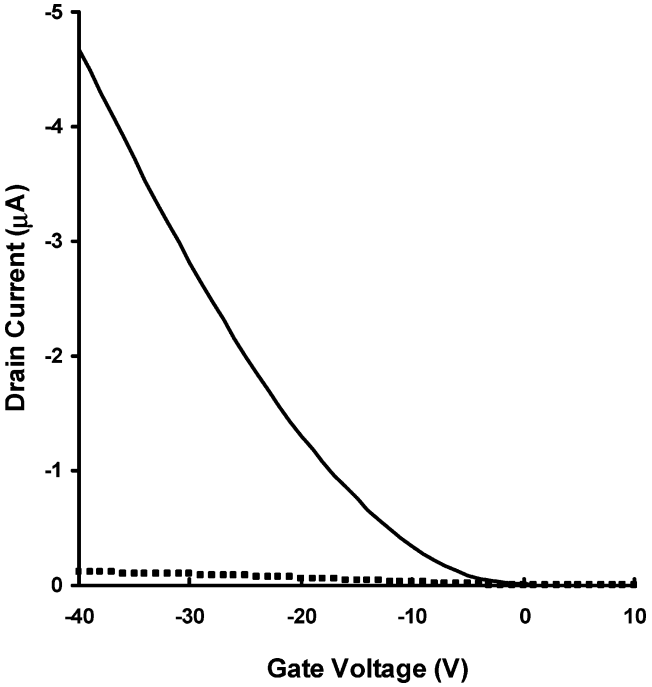

Figure 4. Current−voltage characteristics for coplanar PBTTT-C14 TFTs measured in the linear regime ($V_{sd} = -5$ V) using a thermal oxide dielectric with (solid line) and without (■) an OTS coating. The films were annealed at 180 °C prior to measuring the $I-V$ characteristics. The extracted field effect mobilities were 0.18 cm^2/V s for OTS/SiO_2 and 0.002 cm^2/V s on SiO_2. Source and drain contacts with channel lengths of 20 to 50 μm were made from gold, and the thermal silicon dioxide gate dielectric was 100 nm thick. The supporting doped silicon wafer was used as the gate electrode.

on the slits used for the incident and exiting beam and sample size.[41,42] Due to limitations of time on the beamlines, all types of scans were not performed on all samples.

We used several beamlines and detectors for these experiments so it is important to understand the resolution of each one to best compare complementary data. The resolution of the data obtained with the point detector is collimation on the detector. For the high-resolution specular scattering (beamline 2-1), the collimation was set by a Ta-doped Si-(111) crystal with an angular width of about 0.01°, while, for the high-resolution grazing incidence scattering (beamline 7-2), it was set by 1 mrad Soller slits (effectively 0.1° resolution). The resolution of the data obtained using the image plate detector is coarser than that with the point detector and is determined by the sample size (1.5 cm × 1.5 cm), the distance between the sample and the detector (39.3 cm), and the pixel size (150 × 150 μm^2). The resolution varies as a function of the scattering vector, **q**, but is less than 0.1 $Å^{-1}$ over the range of interest.

For texture measurements of the (200) peaks (e.g., rocking scans) using the image plate detector, we used the following procedure to measure these low Bragg angle (~3°) peaks. An approximate incidence (Bragg) angle was calculated from the position of the (200) peak in the GIXS data. Since this position is only approximate (due to lack of resolution) and we were not confident of the absolute value of the incident angle, we would rock the sample by 0.2° about the nominal (calculated) Bragg angle during the imaging of the scattering. This procedure ensured that we captured the true (200) Bragg diffraction.

Characterization of Morphology. Atomic force microscopy (AFM) was performed on a Digital Instruments Multimode microscope in tapping mode using silicon cantilevers (PointProbe NCH tips from www.nanoworld.com). Fresh tips were used for each sample. The samples were the same as those used in the X-ray scattering experiments. Scanning electron micrographs (SEM) were obtained at PARC.

Results and Discussion

X-ray Scattering from PBTTT Films. We have previously reported initial results on X-ray scattering in thin films of PBTTT.[6] In that report, we assigned a putative unit cell for PBTTT-C12, and we analyze the data here using this assignment. The basic model is shown in Figure 3 where there is lamellar stacking due the alkyl sidechains along the *a*-axis; a π-stacking direction along the *b*-axis; and repeat units of the polymer along the *c*-axis. This basic packing structure is common to many alkylated polythiophenes[28,43] and, as we discuss further, is adequate to understand the basic features of the molecular packing and orientation of the crystalline domains. This assignment of the molecular orientation in the unit cell is consistent with data from NEXAFS measurements on thin films.[44]

X-ray scattering from polycrystalline polymer films is relatively complex due to the combination of disorder and packing defects in the crystalline domains and preferential orientation of these domains, i.e., texturing. It is worthwhile to consider the impact of these effects on the expected X-ray scattering. Before doing this, we establish the coordinate system for the scattering vector **q**: $\mathbf{q_z}$, is defined as the component of **q** perpendicular to the sample surface, while $\mathbf{q_{x,y}}$ is along the sample surface. The in-plane direction of the latter is not important, because the samples are isotropic in plane (vida infra). We will use the lamellar stacking direction, the *a*-axis, as a reference for the orientation of the domains since it is the strongest scattering direction. First, we consider the impact of texturing. If the *a*-axis is highly oriented and perpendicular to the substrate and the unit cell is orthorhombic, its reciprocal lattice vector will be aligned along $\mathbf{q_z}$. We do not expect any texturing within the plane of the film since the films are polycrystalline and cast onto an isotropic OTS/SiO_2 or SiO_2 substrate. In this case, the *b*- and *c*-axes will be randomly oriented in the plane of the substrate, along $\mathbf{q_{x,y}}$. The X-ray scattering pattern for such a film would comprise (*h00*) peaks along $\mathbf{q_z}$, and only (*0kl*) peaks are possible along $\mathbf{q_{x,y}}$. In the case that the *a*-axis is highly aligned parallel to the substrate surface, we would expect the (*h00*) peaks to appear along $\mathbf{q_{x,y}}$ and the (*0kl*) peaks to appear along $\mathbf{q_z}$. The situation is more complex if the films comprise crystalline domains that are relatively misoriented. In the extreme case of no preferential orientation, the X-ray scattering pattern will simply be that of a crystalline powder and comprise diffraction rings. If there is partial preferential orientation, we expect that the scattering pattern will show arcing along constant *q* corresponding to the *d*-spacing of the diffraction peak similar to the diffraction pattern from a fiber of a polymer (Figure 5). If the peaks nominally along $\mathbf{q_z}$ and $\mathbf{q_{x,y}}$ are from the same crystalline domains, then the intensity along the arc defined by the *d*-spacing should have a similar angular intensity profile. In addition to misorientation, the domains may also be defective due to dislocations or other

(42) Toney, M. F.; Wiesler, D. G. *Acta. Crystallogr.* **1993**, *A49*, 624−642.

(43) Yamamoto, T.; Komarudin, D.; Arai, M.; Lee, B.-L.; Suganuma, H.; Asakawa, N.; Inoue, Y.; Kubota, K.; Sasaki, S.; Fukuda, T.; Matsuda, H. *J. Am. Chem. Soc.* **1998**, *120*, 2047−2058.

(44) DeLongchamp, D. M.; Kline, R. J.; Lin, E. K.; Fischer, D. A.; Richter, L. J.; Lucas, L. A.; Heeney, M.; McCulloch, I.; Northrup, J. E. *Adv. Mater.*, in press.

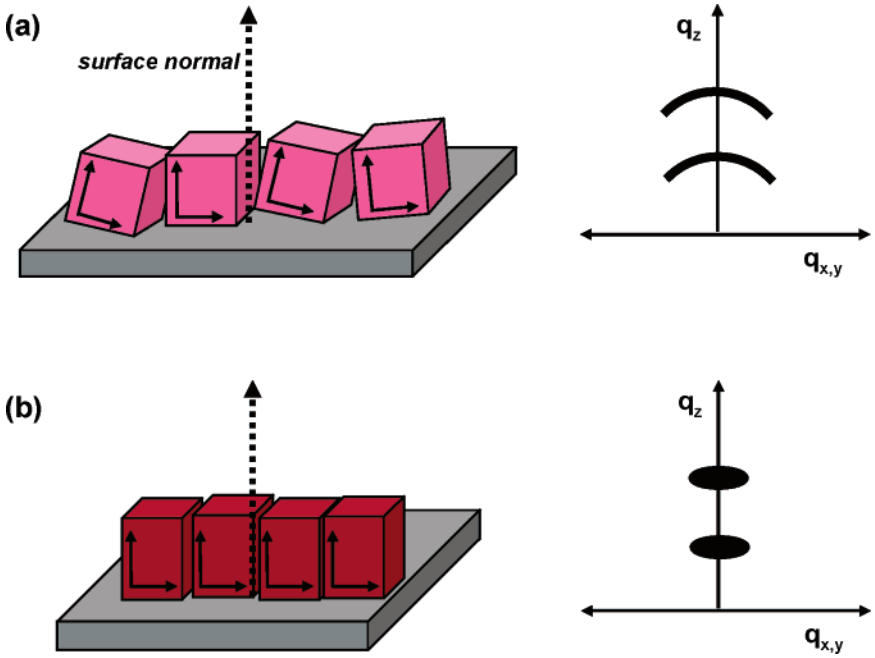

Figure 5. Schematic of crystalline domains and resulting X-ray scattering in a thin polymer film where the arrows represent the unit cell axes of the domain. (a) Domains with the long axis misaligned from the surface normal. (b) Highly aligned domains.

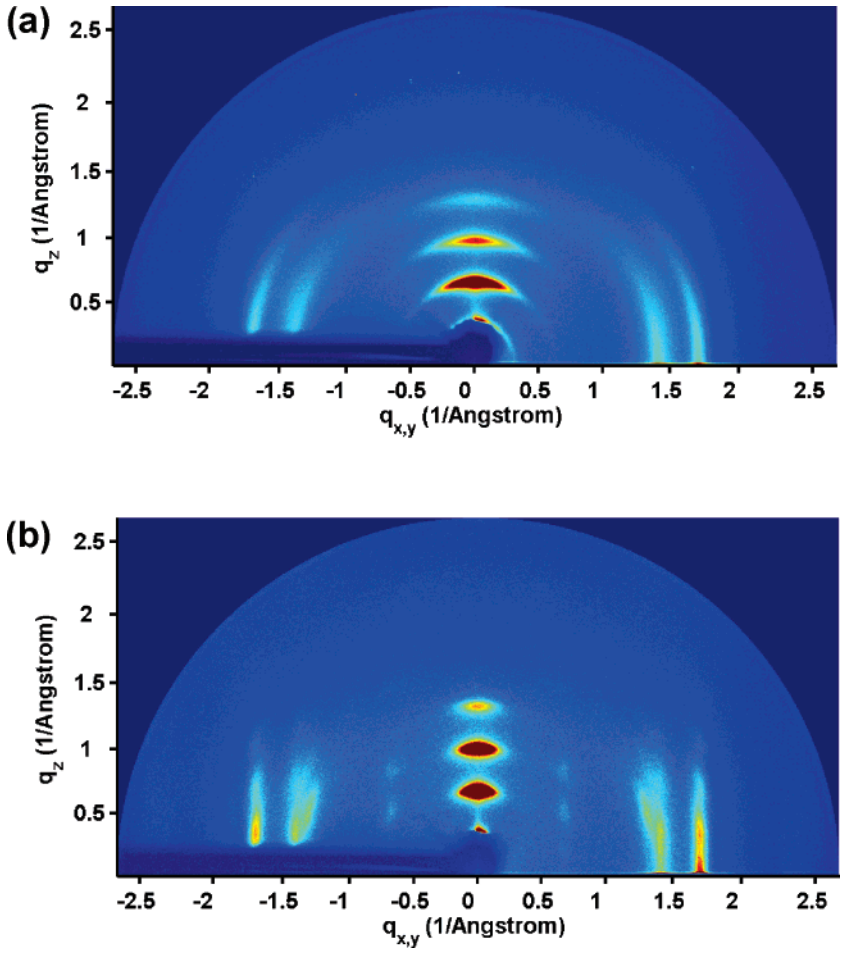

Figure 6. Two-dimensional X-ray scattering at the grazing incidence of a film of PBTTT-C12 (a) as-spun and (b) annealed at 180 °C OTS/SiO_2.

defects. In this case, we would expect to see directional spreading of the scattering, but only close to the diffraction peak, e.g., an elliptical spot with axes aligned to $\mathbf{q_z}$ and $\mathbf{q_{x,y}}$. If the domains are highly defective we also expect not to see the presence of well-resolved peaks with mixed indices, e.g., (*hk*0). In films of PBTTT, we find that these complications are present

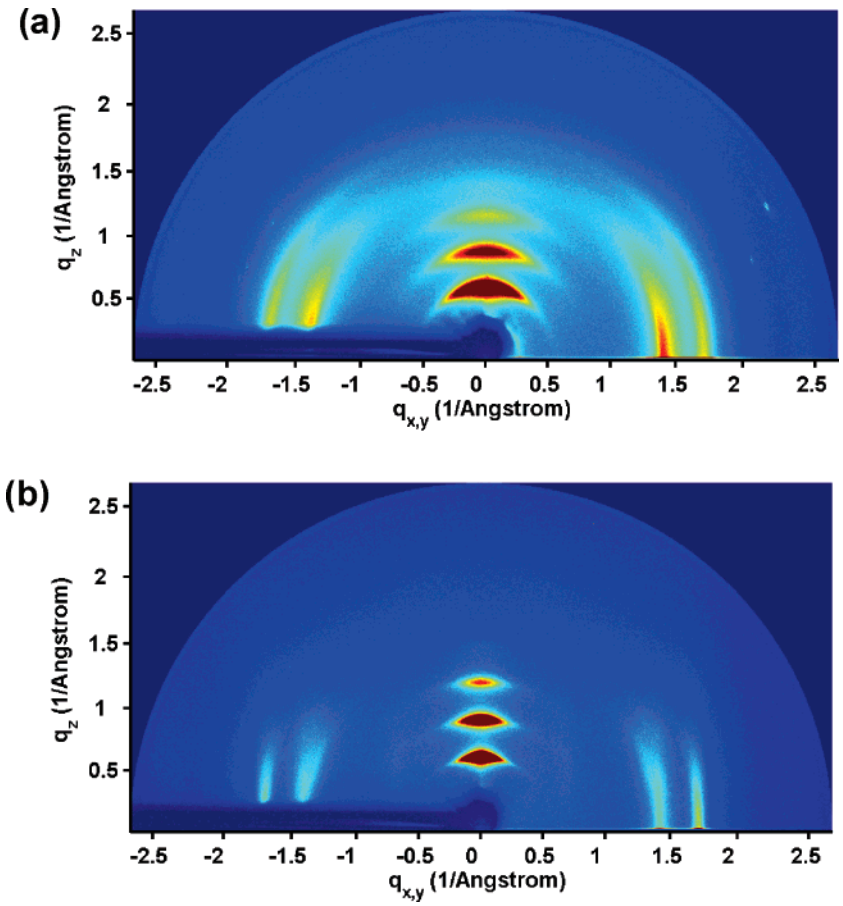

Figure 7. Two-dimensional X-ray scattering at the grazing incidence of a film of PBTTT-C14 (a) as-spun and (b) annealed at 180 °C OTS/SiO_2.

and lead to scattering patterns with simple overall features but a complex detailed structure.

Microstructure of As-Spun Films on OTS/SiO_2. Thin films of PBTTT-C12 and -C14 have preferentially oriented, crystalline domains in their as-spun state on OTS-treated surfaces. Figures 6A and 7A show images of the 2-D X-ray scattering using a grazing incidence geometry beam at ~0.1° incidence for PBTTT-C12 and -C14 on OTS/SiO_2. For both polymers, peaks corresponding to the lamellar spacing are observed along the $\mathbf{q_z}$ direction. These peaks are not fully representative of the Bragg scattering along $\mathbf{q_z}$ because the angle of incidence at the sample is not at the Bragg angle, but they are instead representative of a slice through the reciprocal space intersecting the cone of Bragg scattering (that results from misoriented crystallites).[45] The peaks along $\mathbf{q_{x,y}}$ have been indexed as the (003) and (010) peaks based on the molecular geometry as described previously (Figure 3). The *d*-spacings of the peaks along $\mathbf{q_{x,y}}$ are nearly identical for both the C12 and C14 polymers, while the peaks along $\mathbf{q_z}$ indicate a larger *d*-spacing along the lamellar stack for C14 relative to C12. These data suggest that the materials order in nearly the same way with a simple expansion of the lamellar spacing due to the additional two methylene units in the C14 polymer. The crystalline domains in these films can therefore be considered to have no orientational order in-plane but have strong ordering of the *a*-axis relative to the surface normal.

High-resolution scans were used to determine precisely the *d*-spacings for PBTTT-C12 and -C14 and to examine the orientation of the domains in greater detail. Figure 8 shows the specular scan for PBTTT-C12 where a series of peaks corresponding to the lamellar spacing (*h00*) are observed. The *d*-spacing of the *a*-axis was determined by an average of the peak position for the observed peaks, which for C12 is 19.4 Å and for C14 is 21.0 Å (Table 1).[46] The increase in *d*-spacing

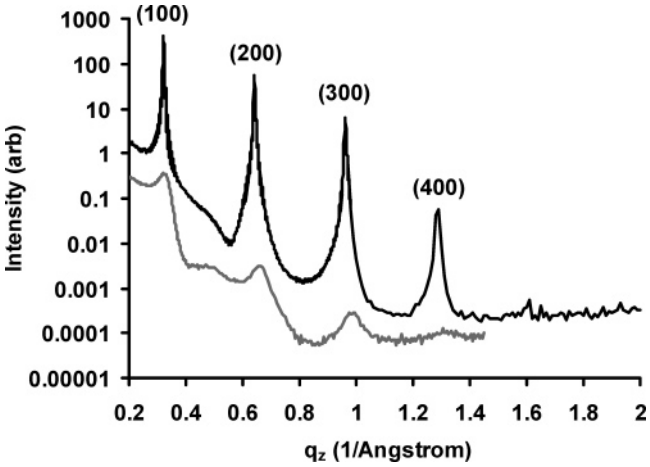

Figure 8. High-resolution specular X-ray scattering from a film of PBTTT-C12 on OTS/SiO_2 as-spun (gray line) and annealed at 180 °C (black line).

(45) In the literature, the fwhm of peaks along $\mathbf{q_z}$ in the grazing incidence is sometimes used to characterize the misorientation of crystalline domains. Although this value represents some measure of the misorientation, it is not fully indicative of the orientation of the domains.

Table 1. Specular X-ray Diffraction Peaks for Samples on OTS-Coated Surfaces

material and annealing condition	index	Q (1/Å)	intensity (arb)	fwhm (1/Å)
		PBTTT-C12		
as-spun	(100)	0.323	0.30	0.040
	(200)	0.659	2.4×10^{-3}	0.048
	(300)	0.985	2.34×10^{-4}	0.060
180° *C*	(100)	0.327	15.3	0.0082
	(200)	0.655	0.953	0.013
	(300)	0.985	0.026	0.015
	(400)	1.315	5.34×10^{-4}	0.022
		PBTTT-C14		
as-spun	(100)	0.292	0.12	0.056
	(200)	0.605	1.64×10^{-3}	0.046
	(300)	0.899	2.94×10^{-4}	0.072
180° *C*	(100)	0.297	8.2	0.008
	(200)	0.593	0.30	0.012
	(300)	0.889	8.54×10^{-3}	0.017
	(400)	1.183	3.54×10^{-4}	0.022

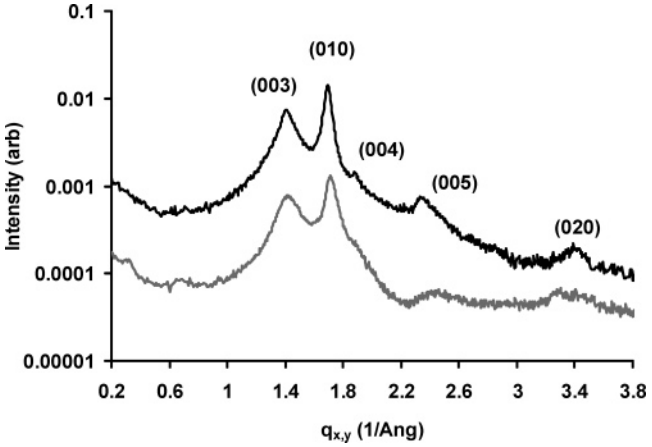

Figure 9. High-resolution grazing incidence X-ray scattering from a film of PBTTT-C12 on OTS/SiO_2 as-spun (gray line) and annealed at 180 °C (black line).

for the C14 compound is expected due to the increase in the alkyl side chain length of two methylene units. The amplitude of the peaks drops exponentially with order. The Debye−Waller factor ($I = I_0 e^{-(q^2\sigma^2)}$), σ^2, is ∼25 Å^2 for both C12 and C14; this value is reasonable and is only slightly larger than the approximate rms roughness of the substrate, ∼2−4 Å.[47] The width of these peaks changes slowly with order implying that the width is dominated by the crystalline domain size rather than a distribution of *d*-spacings for the lamellar stacking.[48,49] The estimated thickness of the domains is ∼300 Å for both C12 and C14, a value significantly smaller than the thickness of the films (∼800 to 1000 Å). We do not observe the (010) peak in these scans suggesting that there are relatively few, if any, domains oriented with the π-stacking direction along the surface normal. High-resolution grazing X-ray scattering measurements of PBTTT-C12 (Figure 9) showed peaks assigned to the π-stacking distance (010) and a progression of peaks that

(46) The *d*-spacing based on the peak positions at low values of $\mathbf{q}_z$ is less certain due to the background from the small angle scattering.
(47) Tidswell, I. M.; Ocko, B. M.; Pershan, P. S.; Wasserman, S. R.; Whitesides, G. M.; Axe, J. D. *Phys. Rev. B* **1990**, *41*, 1111−1128.
(48) Guinier, A. *X-ray Diffraction in Crystals, Imperfect Crystals, and Amorphous Bodies* (1994 reprint ed.); Dover: New York, 1963.
(49) Warren, B. E. *X-ray Diffraction* (1990 reprint ed.); Dover: New York, 1969.

Table 2. Grazing Incidence X-ray Diffraction Peaks for PBTTT-C12

material and annealing condition	index	Q (1/Å)	intensity (arb)	fwhm (1/Å)
		PBTTT-C12		
as-spun on OTS/SiO_2	(010)	1.71	0.0125	0.076
	(020)	3.385	0.0003	0.4
	(003)	1.412	0.0074	0.17
	(004)	1.885	0.001	0.12
	(005)	2.445	0.0003	0.34
180° *C* on OTS/SiO_2	(010)	1.694	0.0130	0.057
	(020)	3.390	0.00013	0.2
	(003)	1.412	0.0068	0.146
	(004)	1.885	0.00055	*0.088*
	(005)	2.348	0.00025	*0.086*
180° *C* on SiO_2	(010)	1.694	0.0180	0.057
	(020)	3.39	0.00028	0.16
	(003)	1.412	0.01	0.136
	(004)	1.89	0.001	*0.128*
	(005)	2.35	0.0007	*0.120*

correlate well with the estimated length of the repeat unit of the polymer, 13.3 Å (Table 2). The presence of weak peaks corresponding to the lamellar repeat distance (100) and (200) are observed in some of the high-resolution grazing scans; these peaks could be due to misoriented crystals in the film or in nonuniform regions near the edge of the sample due to the spin-coating process.

The X-ray scattering from as-spun films of PBTTT-C12 and -C14 indicates that the films contain defective crystalline domains with a distribution of orientations relative to the substrate plane. The specular scattering peaks show a resolution limited peak in rocking scans (Figure 10) suggesting that the crystalline domains nucleate from the interface with OTS/SiO_2.[10] We imaged the Bragg scattering from the (200) peak to determine its relative misorientation to the substrate over a wider range than possible with the high-resolution scans. Although the (200) peak is weaker than the (100) peak, the background scattering near it is significantly weaker than that at the (100) peak. At the Bragg angle, the (200) peak has a strong resolution-limited component at $\mathbf{q}_{x,y} = 0$ with a diffuse background (Figure 11). The diffuse background follows an arc corresponding to the *d*-spacing of the peak with a full-width half maximum (fwhm) of 26° for C12 and a value of 31° for C14. The peaks along the $\mathbf{q}_{x,y}$ axis, (010) and (003), also show significant arcing. The values of the fwhm of the diffuse scattering for C12 are ∼40° for the (003) and (010) peaks with similar values for C14 (Table 3). The general observation that the diffuse scattering is broader for the peaks along $\mathbf{q}_{x,y}$ than those along $\mathbf{q}_z$ is likely due to the contribution of multiple peaks to the total scattering, as there are a large number of rationally indexed spacings at low values (near $q = \sim 1.5$ Å^{-1}) and also due to scattering from disordered regions in the film. Nonetheless, the similarity of the angular distribution of the (200), (010), and (003) peaks supports the interpretation that the arcing is due to a distribution of orientations of the crystalline domains.

Microstructure of As-Spun Films on SiO_2. The X-ray scattering patterns of films of PBTTT spun on bare SiO_2 are similar to those observed for films on OTS/SiO_2 (Figure 12 and Supporting Information). For both C12 and C14, peaks corresponding to the lamellar spacing are observed along $\mathbf{q}_z$ and peaks corresponding to (003) and (010) are observed along $\mathbf{q}_{x,y}$. The

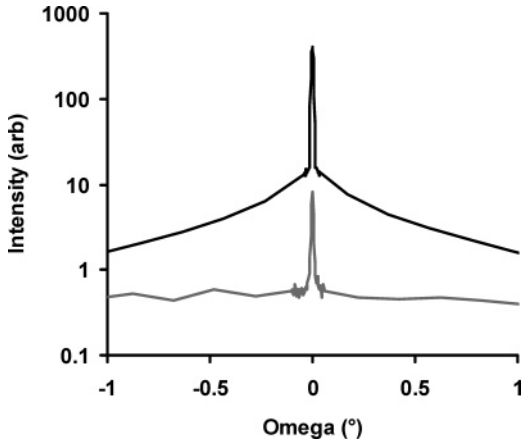

Figure 10. High-resolution rocking curve of the (100) peak from a film of PBTTT-C12 on OTS/SiO_2 as-spun (gray line) and annealed at 180 °C (black line).

d-spacing of the *a*-axis for C12 is 19.6 Å and for C14 is 22.6 Å (Table 4). The *d*-spacing for C12 is nearly identical to that on OTS/SiO_2, but the value for C14 is slightly more than 1 Å larger. The Debye−Waller factor for these peaks is slightly larger than that for films on OTS/SiO_2 and is ∼28 $Å^2$ for both C12 and C14. The *d*-spacing corresponding to the π-stacking direction of the chains is identical on both substrates as is the spacing along the chain direction. The crystalline domains on SiO_2 comprise highly orientated regions and misoriented regions. The fwhm of angular distribution of the diffuse scattering from the (200) peak is about 30° for both C12 and C14. The fwhm of the (010) peak is broader for both C12 and C14 than that of the (200) peak and several degrees broader than that of the (003) peak (Table 3).

Comparison of As-Spun Films on OTS/SiO_2 and SiO_2. These data show that the initial microstructure of films of PBTTT is relatively independent of the nature of the surface that they are spun on. The X-ray scattering for both C12 and C14 show that lamellar planes are highly oriented parallel to the substrate on both SiO_2 and OTS/SiO_2. While the *d*-spacings for both compounds are slightly larger on SiO_2 than those on OTS/SiO_2 these differences are not especially large. If the alkyl sidechains are slightly disordered, then minor conformational changes can lead to changes in spacing of ∼1 Å without disrupting the π-stacking. The nature of the disordered regions that likely exist in these films is not probed by the Bragg scattering in these films so it is possible that the films may differ in the nature of these regions.

The difference in surface energy between SiO_2 and OTS/SiO_2 is not strong enough to disrupt the preferred orientation of the polymer chains in these films. Both substrates show resolution limited peaks for the lamellar peaks suggesting that the films nucleate from the interface with the substrate or are at least more crystalline near the substrate on both SiO_2 and OTS/SiO_2. The spin-coating process is particularly complex for thin films as it involves aggregation of the polymer chains and solvent evaporation. PBTTT exhibits strong aggregation in solution at concentrations larger than a few weight percent at room temperature as evidenced by gelation. If the polymer chains tend to aggregate with π-stacking in solution, their aspect ratio is such than one would expect the lamellar planes to be parallel to the substrate; the polymer molecules then have lengths (∼30 nm) that are comparable to the total thickness of the dried film (∼100 nm). It is also possible that the molecules that aggregate near the substrate have more time to organize prior to complete evaporation of the solvent than those in the bulk leading to better ordering near the substrate interface. This model is qualitatively consistent with the data as the domain size is ∼300 Å, approximately 15 molecular layers, and with the Debye−Waller factor from the scattering of the (*h00*) peaks. It is likely that the thermodynamic driving force of π-stacking along with the preference of forming low energy interfaces drives the orientation of the domains in these films.

Table 3. Misorientation of X-ray Diffraction Peaks for As-Spun Films of PBTTT

material and surface	index	*q* (1/Å)	fwhm (deg)
	PBTTT-C12		
OTS/SiO_2	(200)	0.659	26
	(010)	1.71	39
	(003)	1.412	44
SiO_2	(200)	0.642	30
	(010)	1.71	42
	(003)	1.412	42
	PBTTT-C14		
OTS/SiO_2	(200)	0.605	31
	(010)	1.71	45
	(003)	1.412	59
SiO_2	(200)	0.556	30
	(010)	1.71	54
	(003)	1.412	51

Annealing of PBTTT Films. PBTTT-C12 and -C14 exhibit a liquid crystalline mesophase between 140 °C and the melting temperature near 244 °C for C12 and 248 °C for C14. We have reported previously on how annealing PBTTT in the LC mesophase improves the carrier mobility of TFTs and also dramatically changes the X-ray scattering of thin films.[6] Here we describe the impact of the annealing process on the microstructure of the films in greater detail.

Microstructure of Annealed Films on OTS/SiO_2. Films of PBTTT are highly crystalline after annealing in the LC mesophase. Figures 6B and 7B show the X-ray scattering pattern from PBTTT-C12 and -C14 after thermal annealing at 180 °C for ∼15 min. These films comprise highly oriented and high quality crystalline domains. In comparison to the as-spun films, there is little misorientation of the crystalline domains as observed by the minimal diffuse scattering near the Bragg peaks. For both C12 and C14, the scattering at the (003) and (010) peaks now occurs along a nearly straight line from the position in $\mathbf{q}_{x,y}$ along $\mathbf{q}_z$. For some samples of C12, we have observed the resolution of mixed index peaks for both (*h*10) and (*h*03) (See Table 5).[50] The mixed index peaks have a position in $\mathbf{q}_z$ nearly equal to those of the associated (*h*00) peaks suggesting that the angles β and γ of the unit cell are close to 90°. Although the mixed index peaks for some films of C12 and of C14 are not resolvable, the scattering near the (010) and (003) peaks are well-aligned vertically along $\mathbf{q}_z$. The difference in the scattering between C12 and C14 could be due to the difference in molecular weight of the polymers, differing polydispersity, or the exact time of thermal annealing. No attempt was made to optimize the crystallization conditions for these films so it is

(50) There are also two weak peaks and an arced peak that are difficult to assign using our unit cell. The peak near $\mathbf{q}_{x,y} = 1.31$ $Å^{-1}$, $\mathbf{q}_z = 0.5$ $Å^{-1}$ is not on one of the layer lines of the *a*-axis suggesting that it may correspond to an alternate phase of the material in the film.

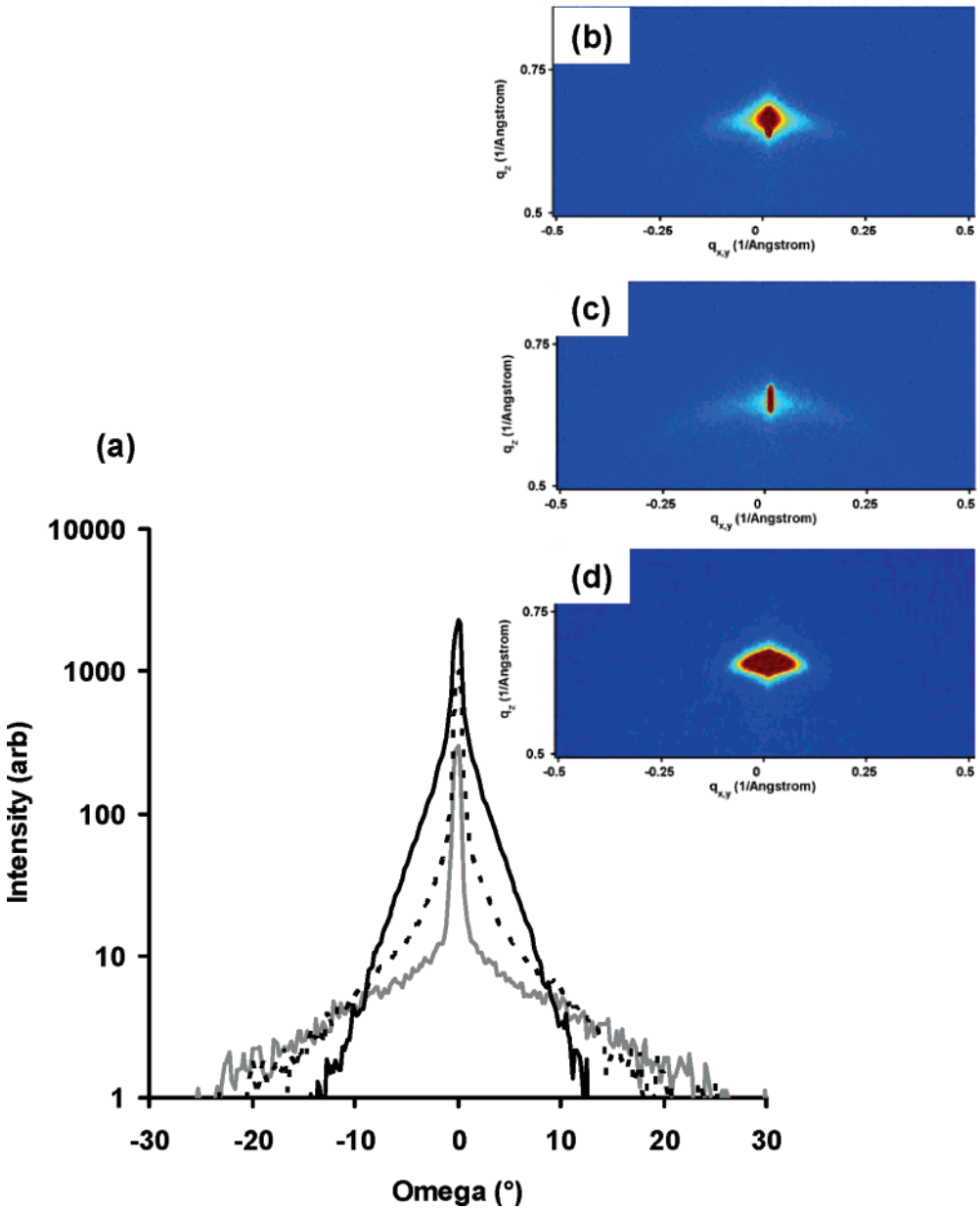

Figure 11. Rocking curves of the (200) reflection using the image plate detector for PBTTT-12 on OTS/SiO_2. (a) Intensity as a function of the rocking angle, ω, from the two-dimensional image plate for the as-spun (gray solid line), annealed at 140 °C (dashed line), and annealed at 180 °C (black solid line). Images of the scattering for (b) the as-spun, (c) annealed at 140 °C, and (d) annealed at 180 °C films are shown in the insets.

unlikely that we have reached a true equilibrium structure in either of these films.

The annealed films show crystalline domains that have high quality and that extend through the entire thickness of the film. High-resolution specular scattering shows a strong increase in intensity upon annealing and substantial narrowing of the peak width relative to the as-spun films. Based on the peak widths, we estimate that the thickness of the domains is ~1000 Å for both C12 and C14 and is comparable to the total thickness of the film (~800−1000 Å). The *d*-spacing for C12 is 19.2 Å and that for C14 is 21.2 Å, consistent with the longer alkyl side chain length in C14. The Debye−Waller factor for these films is ~23 $Å^2$. High-resolution rocking curves show a similar resolution limited peak as that of the as-spun films suggesting that the crystalline domains are highly oriented from the substrate surface (Figure 10).

High-resolution grazing incidence scattering that was collected for the C12 films shows the same features as those for the lower resolution 2-D data. Due to larger dynamic range, we also observe the (020), (004), and (005) peaks (Figure 8). Interestingly, the width of the peaks decreases with annealing and the intensity increases slightly, but the total area of these peaks remains roughly constant. One possible explanation for this observation is that the peaks in the as-spun films represent an aggregate of the main peak and mixed index peaks, e.g., (010) and (110), (210), etc., due to the misorientation of the domains, but only represent the main peak, e.g., (010), after annealing. The π-stacking distance does not change appreciably upon annealing suggesting that the main effect of annealing is to modify the lamellar stacking and to improve ordering along the *b*- and *c*-axes.

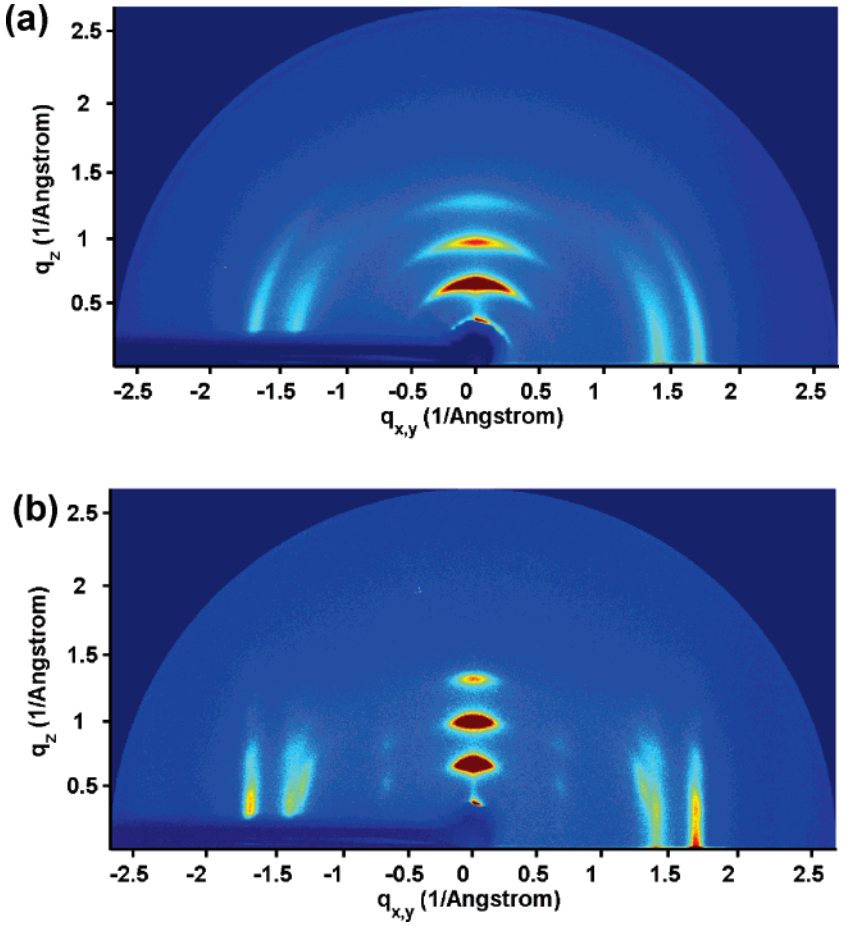

Figure 12. Two-dimensional X-ray scattering at the grazing incidence of a film of PBTTT-C12 on SiO_2 (a) as-spun and (b) annealed at 180 °C.

Table 4. Specular X-ray Diffraction Peaks for Samples on Bare SiO_2 Surfaces

material and annealing condition	index	*Q* (1/Å)	intensity (arb)	fwhm (1/Å)
		PBTTT-C12		
as-spun	(100)	0.320	0.280	0.072
	(200)	0.642	0.012	0.080
	(300)	0.982	1.6×10^{-4}	0.070
180° C	(100)	0.325	1.4	0.0084
	(200)	0.652	4.6×10^{-2}	0.017
	(300)	0.980	2.3×10^{-3}	0.020
	(400)	1.309	1.0×10^{-4}	0.041
		PBTTT-C14		
as-spun	(100)	0.279	0.27	0.088
	(200)	0.556	0.031	0.080
	(300)	0.834	3.0×10^{-5}	0.120
180° C	(100)	0.291	0.476	0.009
	(200)	0.584	0.020	0.013
	(300)	0.880	1.6×10^{-3}	0.018
	(400)	1.176	1.4×10^{-4}	0.038

To understand the effects of thermal annealing, we examined films annealed at 140 and 180 °C to examine how the crystalline domains change their orientation. We used the (200) peak to probe the orientation of the crystalline domains using the imaging capability of the 2-D detector. Figure 11 shows the rocking curve of PBTTT-C12. The (200) peak shows a resolution limited central feature for all three films. The diffuse region of the scattering changes strongly as a function of temperature. It is clear that the shape of the diffuse scattering changes with annealing at 140 °C and narrows. The shape of the peak changes dramatically for films annealed at 180 °C, and they are not well-described as arced peaks. The profile of the peak is elliptical in reciprocal space and is spread relatively broadly along $\mathbf{q}_{x,y}$. This peak profile suggests that the domains are highly oriented with defective regions more similar to those of a layered inorganic material than a typical polymeric film. These defects are likely due to dislocations of the polymer chains as they stack within a crystalline domain.

Microstructure of Annealed Films on SiO_2. The X-ray scattering patterns for annealed PBTTT films on SiO_2 have essentially the same features as those on OTS/SiO_2. The X-ray scattering from both C12 and C14 annealed at 180 °C on SiO_2 is more intense relative to the as-spun film particularly along the specular direction, $\mathbf{q}_z$. The X-ray scattering shows vertically oriented peaks along $\mathbf{q}_z$ at points along $\mathbf{q}_{x,y}$ near the (003) and (010) peaks for both C12 and C14. For some samples of C12, mixed index peaks can be resolved that index to (*h*10) and (*h*03) peaks. High-resolution specular scans show that the crystalline domains are highly oriented and extend through the thickness of the film. The *d*-spacing for C12 is 19.25 Å and that for C14 is 21.50 Å, consistent with the longer alkyl side chain length in C14. The Debye−Waller factor for these films is ~24 Å^2. The crystalline domains extend through the thickness of the film based on the width of these peaks for both C12 and C14. Rocking scans for the lamellar peaks show resolution-limited peaks with a smaller diffuse background. The in-plane structure of C12 was examined using grazing incidence scattering. These

Table 5. X-ray Diffraction Peaks from Grazing Incidence Scattering of Films of PBTTT-C12 Annealed at 180 °C

$q_{x,y}$ (1/Å)	q_z (1/Å)	index	intensity (arb)
0.67	0.51		0.16
0.67	0.82		0.24
1.41	0	(003)	2.00
1.41	0.37	(103)	1.45
1.41	0.70	(203)	0.69
1.41	1.06	(303)	0.19
1.31	0.50		0.80
1.70	0	(010)	6.00
1.70	0.37	(110)	1.38
1.70	0.69	(210)	0.70
1.70	1.07	(310)	0.09

scans showed the same features along $\mathbf{q}_{x,y}$ as the 2-D detector and allowed for the resolution of the (020), (004), and (005) peaks.

Comparison of Annealed Films on OTS/SiO_2 and SiO_2. The microstructure of crystalline domains of films on both OTS/SiO_2 and SiO_2 is substantially similar. The crystalline domains have the same unit cell independent of the interfacial layer, and the texturing of these domains is nearly identical. The width of the specular peaks is narrow and suggests that the crystalline domains extend through the entire thickness of these films for both substrates. The *d*-spacing of lamellar stacking is nearly identical on both substrates after annealing, unlike the as-spun films. This observation is consistent with the interpretation that the microstructure of the as-spun films is kinetically limited, but the polymer chains crystallize in essentially the same structure after annealing at a temperature that allows the polymer chains to reorganize and remove defects. The two substrates have similar roughnesses (rms ~2−4 Å), so it is not surprising that the crystalline regions are highly oriented with good lateral coherence on both. No differences in the π-stacking distances are observed as well. The X-ray scattering, of course, does not probe the disordered regions in these films that exist between crystalline grains, so these regions could be different in the films. We also have not carefully investigated the structure of the packing defects in these films, because of the complicated (and likely ambiguous) nature of the scattering from the defects.

How Do the Structures of Films of PBTTT on OTS/SiO_2 and SiO_2 Differ? The lateral dimensions of the crystalline grains of PBTTT depend on interfacial chemistry. Atomic force micrographs show that films on OTS/SiO_2 of C12 form relatively large (~200 nm), rectangular, flat domains whereas those on SiO_2 show smaller (~50−100 nm) granular grains (Figure 13). Large depressions are observed in films of PBTTT-C12 after annealing in the AFM images. Scanning electron micrographs show that these depressions do not extend to the bottom of the substrate (Supporting Information). Such depressions were not observed in the annealed samples on SiO_2. This morphology suggests that PBTTT is dewetting from the substrate to form larger domains on OTS/SiO_2 relative to SiO_2. The adhesion between PBTTT on OTS/SiO_2 is relatively poor in comparison to SiO_2, suggesting that the difference is likely due to the surface mobility of the polymer chains on these interfaces. Additionally, the sidechains of the PBTTT molecules should have more favorable energetic interactions with the OTS layer than the silanol groups on bare SiO_2. The specular scattering data show that despite the difference in size, these grains are well-ordered through their thickness and the lamellar

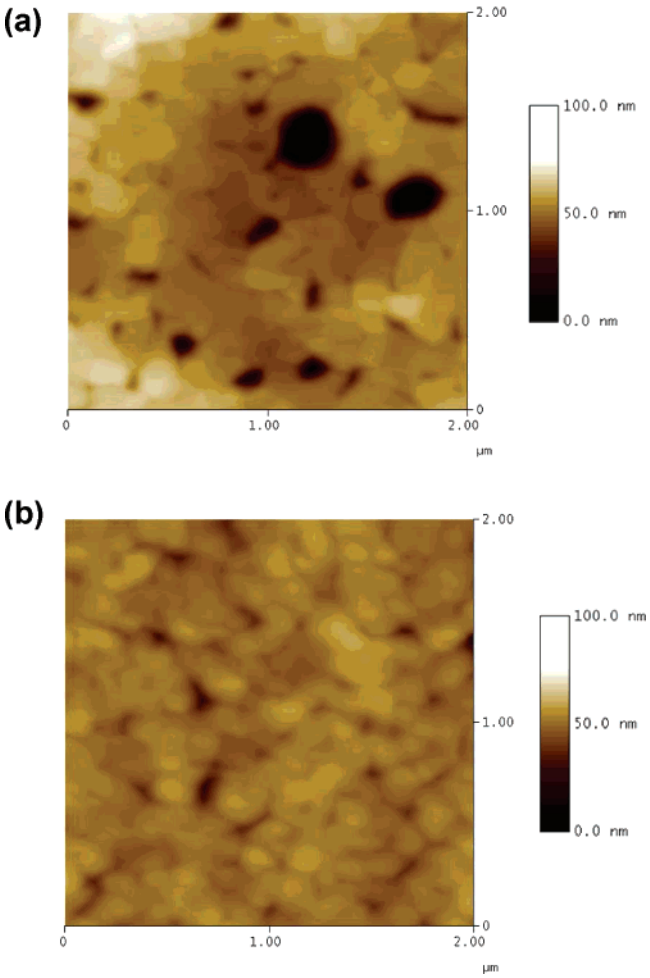

Figure 13. Atomic force micrographs of films of PBTTT-C12 annealed at 180 °C on (a) OTS/SiO_2 and (b) SiO_2.

layers are well-correlated laterally due to the low roughness of the substrate. Differences in grain structure based on AFM phase images have been reported for films of poly(3,3′-didodecylquaterthiophene), PQT-12, on OTS/SiO_2 and SiO_2, but the topographic differences are more subtle than those seen here.[51]

Why Do Films of PBTTT on OTS/SiO_2 and SiO_2 Have Different Carrier Mobilities? The main difference between films of PBTTT on OTS/SiO_2 and SiO_2 surfaces is the aerial size of the crystallites with the former being approximately a factor of 2 larger on a side than the latter. Increasing the number of grain boundaries increases the interfacial area of contact of the crystalline regions with defective or disordered regions. This poor continuity of the crystalline domains is likely to be part of the cause of the difference in field-effect mobility observed on these two surfaces (>0.1 cm^2/V s on OTS/SiO_2 and <0.005 cm^2/V s on SiO_2). A percolation model has been proposed that explains carrier transport through a polymeric polycrystalline film as conduction through a series of crystalline domains and disordered regions.[52] The ordered regions comprise molecules with larger conjugation lengths and better intermolecular electronic coupling than the chains in the disordered regions; this difference leads to regions with different effective bandgaps. The carriers in the ordered regions have to tunnel or hop through

(51) Wu, Y.; Liu, P.; Ong, B. S.; Srikumar, T.; Zhao, N.; Botton, G.; Zhu, S. *Appl. Phys. Lett.* **2005**, *86*, 142102.
(52) Street, R. A.; Northrup, J. E.; Salleo, A. *Phys. Rev. B* **2005**, *71*, 165202.

the disordered regions in order to move through the film. The fraction of area of the film that is disordered can be estimated to be at least twice as large for films on SiO_2 relative to OTS/SiO_2, based on a simple model where each grain is surrounded by a thin disordered layer. Such a difference is likely to dramatically change the percolation path of carriers in these films suggesting an origin for the difference in mobility. Probing the nature of the disordered regions is challenging for any spectroscopic technique. An estimate of the size of these regions based on the AFM images is <1% of the total volume of the film; few spectroscopic techniques have the ability to separate mixtures of different populations at this level.

Conclusions

We have shown how the microstructure of PBTTT is affected by interfacial chemistry and by thermal annealing. PBTTT forms highly ordered crystalline domains on both SiO_2 and OTS/SiO_2 surfaces. As-spun films have crystalline domains that are relatively defective and misoriented relative to the substrate. The as-spun domains begin to reorient and expand in the lamellar dimension as the films are annealed in the LC phase beginning at 140 °C. Large crystalline domains form at temperatures near 180 °C in short times (minutes). The orientation and molecular packing structure of these domains on both OTS-treated and bare SiO_2 are similar. The domain sizes on these substrates differ laterally as observed by their topography in AFM micrographs. These results are likely due to the presence of different nucleation densities or surface mobilities of the polymer molecules on these surfaces.

These results demonstrate that while the orientation and molecular packing in films of semiconducting polymers have an impact on field-effect mobility of charge carriers, the connection is not a simple one. For P3HT, large differences in mobility have been attributed in part to the orientation and connectivity of crystalline domains.[5,21] This connection is not absolute as films of PBTTT have similar crystalline structures and orientations on both OTS/SiO_2 and SiO_2 yet have very different carrier mobilities. Small concentrations of trap states formed by disordered molecules (~1 ppt or less) can have a large impact on transport. In a TFT, only the first several molecular layers contribute to transport, whereas X-ray scattering experiments generally probe the entire film so it is not possible to conclude that the observed molecular ordering is the only cause of the difference in transport properties.

Acknowledgment. Portions of this research were carried out at the Stanford Synchrotron Radiation Laboratory, a national user facility operated by Stanford University on behalf of the U.S. Department of Energy, Office of Basic Energy Sciences. The authors thank Alberto Salleo (Stanford) and John Northrup, William Wong, and TseNga Ng (PARC) for helpful discussions.

Supporting Information Available: Additional experimental data including plots of high-resolution specular, grazing incidence, and 2-D X-ray scattering for some samples of PBTT-C14, rocking curves of PBTTT-C14, and a scanning electron micrograph of the morphology of an annealed film of PBTTT-C12. This material is available free of charge via the Internet at http://pubs.acs.org.

JA0670714